Optoelectronics Reports 2024, 1(1), 283.
https://doi.org/10.59400/oer.v1i1.283

Article

Exploring the efficiency and transparency in toxic and non-toxic perovskite solar cells by using SCAPS-1D

Abdul Haseeb Hassan Khan[1,2,†], Hameed Ullah[2,†], Liping Li[2], Abdul Basit[1], Khadija Boughanbour[3], Sumayya Khan[4], Aimal Daud Khan[1,*]

[1] U.S.-Pakistan Center for Advanced Studies in Energy, University of Engineering and Technology, Peshawar, 25120, Pakistan
[2] Electronic and Communication Engineering, Anhui University, Hefei 230093, Anhui Province, China
[3] Polydisciplinary Faculty, Ibn Zohr University, Agadir 80000, Morocco
[4] Health Care Administration, Northeastern University, Boston, MA 02115, USA
*** Corresponding author:** Aimal Daud Khan, aimaldawoodkhan@gmail.com
† First and second author contributed equally.

CITATION

Khan AHH, Ullah H, Li L, et al. Exploring the efficiency and transparency in toxic and non-toxic perovskite solar cells by using SCAPS-1D. Optoelectronics Reports. 2024; 1(1): 283. https://doi.org/10.59400/oer.v1i1.283

ARTICLE INFO

Received: 32 October 2023
Accepted: 5 December 2023
Available online: 9 January 2024

Abstract: In the quest for sustainable energy solutions, we undertook a rigorous examination of both toxic and non-toxic perovskite solar cells (PSCs), assessing their potential across different absorber thicknesses and their viability within Building-Integrated Photovoltaics (BIPV). Our $MAPbI_3$-based solar cell, utilizing TiO_2 and Cu_2O as electron and hole transport layers, respectively, exhibited an efficiency of 20.65% with a 400 nm opaque absorber. Interestingly, when this thickness was reduced to 200 nm, endowing the PSC with semitransparent properties, certain performance metrics altered, revealing insights crucial for BIPV integration. Further experiments with the toxic $FAPbI_3$ absorber resulted in an efficiency of 23.37% for its 400 nm opaque variant. However, the semitransparent 200 nm layer presented distinct characteristics, emphasizing the complex interplay between thickness, transparency, and efficiency. Our exploration did not stop at toxic materials; we delved into non-toxic alternatives, $MAGeI_3$ and $RbGeI_3$. These variants produced efficiencies of 14.59% and 20.40% for their 400 nm configurations. Yet again, their 200 nm semitransparent counterparts showcased performance nuances. Synthesizing our findings, it becomes evident that semitransparent PSCs hold significant promise for BIPV applications, but achieving an optimal blend of efficiency, transparency, and architectural appeal demands further focused research.

Keywords: semitransparent; opaque; toxic perovskite solar cell; non-toxic perovskite solar cell; BIPV

1. Introduction

Organometal trihalide perovskites quickly became known as a potential category of absorbing materials for extremely efficient solar cells [1–3]. Their success may be attributed to factors such as their ideal band gap for methylammonium lead iodide, $CH_3NH_3PbI_3$) and elevated absorbance coefficients [4], as well as lengthy carrier diffusion lengths [5,6]. Furthermore, perovskite solar cells (PSCs) may be manufactured using simplified solution-based technologies that are readily adaptable to constant, high quantities operations [7–9].

During the past few years, perovskite-based solar cells have significantly improved their power conversion efficiency (PCE), with values above 25% [10]. Potentially a result, perovskite solar cells are seen as a strong contender for substituting the conventional, Si-based solar cells that now control the photovoltaic (PV) industry. The molecular structure for perovskite is ABX3, wherein A is a

monovalent cation (e.g., methylammunium, formammidinium, or Cs), B is a divalent rare metal (Pb or Sn), and X is a halide anion (I, Br, or Cl) [11–15]. Perovskite has distinct optic and electrical features, including a high attenuation ratio [16,17] as well as a direct along with configurable band gap [18–20]. Within these benefits is the fact that this perovskite manufacturing procedure is centered on a solution process, which allows for a number of very simple depositing processes like as spin coating, screen printing, as well as evaporation [21–24]. In recognition of the appealing qualities of perovskite primarily band gap tuning and varied solar cell topologies, semitransparent solar cells may be created in which some light passes through the cells and some is absorbed via the energy-harvesting layer. Transparency may be produced by either creating a thin perovskite layer or partially covering the perovskite, leaving sections of the transparent substrate unfilled. Furthermore, by adjusting the band gap, the transparency may be adjusted. Semitransparent photovoltaic cells may be used as glass in constructions and tall buildings, giving both shade and green power. In the year 2018, both the residential and commercial sectors comprised over 40% of total U.S. energy consumption. while energy from renewable resources contributed for around 11% of the entire US consumption of energy and approximately 17% of the nation's electricity production [25]. By generating electricity while relying on the power grid, building integrated photovoltaic (BIPV) systems may considerably cut buildings energy usage and greenhouse gas emissions. Furthermore, most traditional solar cells are mainly situated on roofs or in open areas that have the greatest exposure to sunlight, whereas semitransparent solar cells can be integrated into the sides of the building and thus optimize space capacity and thus generate power.

The incorporation of semitransparent solar cells into various architectural elements such as building facades, ceilings, roofs, windows, fences, walls, and awnings presents a viable and economically efficient approach to utilizing the surface area of buildings. This strategy has the potential to enhance the overall installed capacity in densely populated urban areas and enable the delivery of electrical energy in close proximity to the areas of consumption [26]. Currently, efficient crystalline silicon solar cells, which are nontransparent, are widely used for building ceilings and roofs. On the other hand, semitransparent solar cells made from amorphous Si (a-Si) and polymers have seen limited application in areas like windows, facades, fences, and awnings, partly due to the restricted range of brown and red colors they offer [27]. Semitransparent solar cells with building-integrated photovoltaic (BIPV) must have good bifacial efficiency and significant color tunability. When juxtaposed with a monofacial cell, simultaneous collection of direct and diffused/reflected light results in better power conversion efficiencies (PCEs). This is particularly relevant when semitransparent solar cells are mounted atop solar awnings, whereby light may be gathered from various angles from dawn to sunset, as well as through solar reflection albedo (RA). Furthermore, vibrant, semitransparent solar cells featuring extensive color tunability that does not restrict power conversion are essential for designing energy-efficient and aesthetically pleasing structures. Flexible, successful bifacial colorful semitransparent solar cells must have three main components: (i) a highly transparent rear electrode and interlayers to ensure high bifacial light transmission and efficiency; (ii) a good refractive index correspond to among all semitransparent solar

cell interlayers to create strong light interference to form distinct colors; and (iii) a simple and cost-effective fabrication process.

Perovskite solar cells (PSCs) have become known as a promising choice for semitransparent solar cells due to their ability to achieve PCEs of more than 24% and 18.1% for opaque and semitransparent PSCs (ST-PSCs), accordingly, while maintaining low manufacturing costs [3,28–30]. Semitransparent-PSCs feature a bifacial structure that allows them to gather either direct as well as reflected radiation at the same time [31,32]. A potential way for achieving semitransparency involves keeping the concentration of bromide (or iodide) constant while manipulating the thickness of the film by altering the solution concentration [22]. In order to achieve maximum absorbance, a perovskite film thickness of 400 nm is required [33]. The average thickness of the semitransparent perovskite film is approximately 200 nm, which is less than the usual thickness of high-efficiency perovskite films, ranging from 500 to 700 nm [34]. A reduction in the thickness of the perovskite film will result in the transmission of a portion of the incident light, as determined by its absorption coefficient, which is contingent upon the wavelength. As mentioned earlier, the prevailing approach for producing semitransparent perovskite solar cells involves the reduction of film thickness through the utilization of a perovskite solution with minimal concentration.

In this research, our detailed simulation using the SCAPS-1D tool shed light on the distinct properties and performances of both toxic ($MAPbI_3$ and $FAPbI_3$) and non-toxic ($MAGeI_3$ and $RbGeI_3$) perovskite solar cells. By examining these compounds at the specified thicknesses of 400 nm and 200 nm, serving as opaque and semitransparent absorbers respectively, we unraveled the intrinsic nuances that define their behavior. Our choice of TiO_2 for the electron transport layer (ETL) and Cu_2O for the hole transport layer (HTL) was underpinned by their renowned synergistic electronic characteristics and proven harmony with perovskite structures. Through the juxtaposition of the photo-physical and electronic attributes of these perovskites under the defined scenarios, we have unveiled pivotal insights. These findings not only underscore pathways to heightened efficiency in perovskite solar cells but also emphasize the paramount importance of safety and environmental sustainability.

2. Methodology

2.1. Solar cell structure

The design of the solar cell presented in **Figure 1** is carefully engineered to optimize photovoltaic performance through the strategic selection of materials for each functional layer. The electron transport layer (ETL) is composed of titanium dioxide (TiO_2), a wide bandgap semiconductor known for its high electron mobility and chemical stability. The large bandgap of TiO_2 ensures that it is transparent to the visible spectrum, allowing photons to reach the absorber layer unimpeded. Its electron mobility is critical for the rapid extraction and transport of electrons from the absorber layer to the electrode, thus minimizing the chance of electron-hole recombination within the perovskite layer. The hole transport layer (HTL) utilizes copper (I) oxide (Cu_2O), selected for its p-type semiconductor characteristics and its energetic

alignment with the valence band of the perovskite materials. Cu_2O's favorable band energetics promote efficient hole extraction from the absorber layer. The holes, once generated, find a lower energy state in the Cu_2O layer, which serves as a driving force for their swift transport to the electrode. This ensures a unidirectional flow of charge carriers, which is essential for reducing recombination and improving the overall cell efficiency. At the heart of the solar cell lies the absorber layer, composed of either toxic perovskites, $MAPbI_3$ and $FAPbI_3$, or their non-toxic counterparts, $MAGeI_3$ and $RbGeI_3$. These materials are chosen for their ability to absorb a broad spectrum of light and their suitable bandgap energies, which ensure the generation of electron-hole pairs upon exposure to sunlight. The absorber layer's material composition is critical as it defines the wavelength range of photon absorption and the potential photogenerated current. The solar cell structure showcases two absorber layer thicknesses, each serving a unique application purpose. The thinner, 200 nm configuration provides a balance between light absorption and transparency, making it suitable for building-integrated photovoltaics (BIPV) where semi-transparency is desired for aesthetic or functional reasons, such as in windows that also generate power. In contrast, the thicker, 400 nm absorber layer is designed for maximum energy conversion. The increased thickness enhances the probability of photon absorption as it offers a longer path length for the photons, thereby increasing the chance of interacting with the perovskite material. This is particularly beneficial for stand-alone power generation applications where high efficiency is paramount.

Each layer of the solar cell contributes to its overall efficiency. The TiO_2 ETL and Cu_2O HTL are not only responsible for charge transport but also for establishing an internal electric field due to their respective n-type and p-type doping levels. This field is crucial for the drift of charge carriers towards their respective electrodes. The perovskite layer's role is multifaceted: it must absorb photons to create charge carriers, permit the dissociation of these carriers into free electrons and holes, and allow their initial transport towards the ETL and HTL. The solar cell's layered structure, incorporating TiO_2 and Cu_2O as transport layers and perovskite materials as absorbers, is a carefully optimized system. Each component is selected to enhance light absorption, charge generation, and separation while minimizing recombination, thus ensuring efficient energy conversion. The variable absorber layer thickness further fine-tunes the cell's application towards either BIPV or maximum power output scenarios.

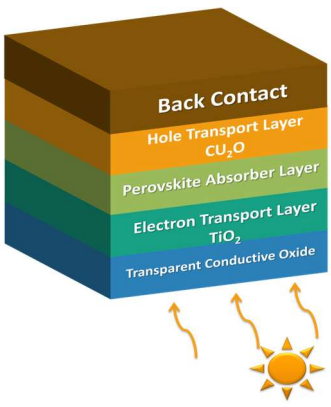

Figure 1. PSC structure.

2.2. Simulation methodology

The SCAPS-1D simulation program, developed by the University of Ghent in Belgium, was used for this work [35]. The primary basis for the numerical calculations performed within SCAPS-1D consists of three essential equations, namely the Poisson equation, the electron continuity equation, as well as the hole continuity equation.

Equation of continuity for electrons:

$$\frac{\partial_n}{\partial_t} = \frac{1}{q}\frac{\partial J_n}{\partial_x} + G_n - R_n \tag{1}$$

Equation of continuity for holes:

$$\frac{\partial_P}{\partial_t} = \frac{1}{q}\frac{\partial J_p}{\partial_x} + G_p - R_p \tag{2}$$

Poisson's equation:

$$= -\frac{\partial}{\partial x}\left(-\varepsilon(x)\frac{\partial V}{\partial x}\right) \tag{3}$$

$$= q[p(x) - n(x) + N_D^+(x) - N_A^-(x) + P_t(x) - n_t(x)] \tag{4}$$

R_p = hole recombination rate, q = charge, R_n = electron recombination rate, ε = dielectric permittivity, G_p = generation rate of holes, V = potential, G_n = generation rate of electrons , $p(x)$ = concentration of unattached holes, J_p = hole current density, $n(x)$ = concentration of unattached electrons, J_n = electron current density, $N_D^+(x)$ = Ionised donor concentration, $n_t(x)$ = electron trap density trap density, $N_A^-(x)$ = Ionised acceptor concentration, $P_t(x)$ = hole traps density

The SCAPS-1D software enables the design to develop a heterostructure solar cell with the potential to incorporate up to seven distinct layers. This software also facilitates the simulation of electron and optics properties of functional thin films within the solar cell, allowing for analysis across multiple variables. The photovoltaic-structure configuration consists of several components, including titanium dioxide (TiO_2) as the electron transport layer (ETL), and various light-absorbing materials such as methylammonium lead iodide ($MAPbI_3$), formamidinium lead iodide ($FAPbI_3$), methylammonium germanium iodide ($MAGeI_3$), and rubidium germanium iodide ($RbGeI_3$). Additionally, copper (I) oxide (Cu_2O) serves as the hole transport layer (HTL). The aforementioned structure of PSC is employed in the preliminary simulation. The input parameters of the initial structure, as presented in **Table 1**, are derived from theoretical frameworks and prior academic publications [36–39].

For our simulations, an illumination intensity of 1000 Wm^2, mimicking the standard AM 1.5G solar spectrum, was maintained, with the ambient conditions set at a temperature of 300 K. Electron and hole thermal velocities were standardized at 10^7 cm/s, ensuring consistent transport dynamics across the studied structures. To render a more nuanced and realistic model of perovskite solar cells (PSCs), interface layers were judiciously incorporated: both at the TiO_2/absorber junction and the absorber/Cu_2O interface. This approach captures the potential electronic and optical interactions at these critical junctions. Furthermore, a neutral defect density was assumed for all interface layers, aligning with the premise of idealized device structures. The doping profiles of our simulations were guided by a combination of predetermined and variable parameters. Acceptor doping concentration (NA) was varied based on both the intrinsic properties of the materials under investigation and

extant literature data. A pivotal aspect of our study entailed manipulating the absorber layer's thickness and doping concentration, both for semitransparent and opaque configurations. By systematically varying these parameters, to discern the inherent relationships between structural dimensions, material doping, and resulting photovoltaic characteristics, especially when transiting between opaque and semitransparent solar cell regimes. This detailed investigation aspires to elucidate the nuanced interplay of factors influencing the performance of PSCs in both optical configurations.

Table 1. The input parameters for the initial device configuration in the SCAPS-1D.

Properties	**TiO_2**	**$MAPbI_3$**	**$FAPbI_3$**	**$MAGeI_3$**	**$RbGeI_3$**	**Cu_2O**
Thickness (nm)	150	450/200	400 /200	400/200	400/200	150
Bandgap (eV)	3.2	1.550	1.510	1.900	1.310	2.170
Electron affinity (eV)	3.9	3.9	4	3.980	3.9	3
Dielectric permittivity (relative)	32	6.5	6.6	10.000	23	7.5
CB effective density of states	2×10^{18}	2.2×10^{18}	1.2×10^{19}	1×10^{16}	1.4×10^{19}	1.1×10^{19}
VB effective density of states	1.8×10^{19}	1×10^{18}	2.9×10^{18}	1×10^{15}	2.8×10^{19}	2×10^{19}
Electron thermal velocity	1×10^{7}	1×10^{7}	1×10^{7}	1×10^{7}	1×10^{7}	1×10^{7}
Hole thermal velocity	1×10^{7}	1×10^{7}	1×10^{7}	1×10^{7}	1×10^{7}	1×10^{7}
Electron mobility	2×10^{1}	2	2.7	1.620×10^{1}	2.8×10^{1}	2.1×10^{2}
Hole mobility	1×10^{1}	2	1.8	1.01×10^{1}	2.7×10^{1}	8.0×10^{1}
Shallow uniform donor density (ND)	1×10^{17}	-	1×10^{16}	1×10^{19}	1×10^{9}	-
Shallow uniform acceptor density (NA)	-	1×10^{17}	1×10^{16}	1×10^{19}	1×10^{9}	2×10^{19}
Defect density	1×10^{15}	1×10^{14}	1×10^{14}	1×10^{14}	1×10^{15}	1×10^{15}
Interface defects	1×10^{10}	-	-	-	-	1×10^{15}

3. Result and discussion

3.1. Performances analysis of semitransparent and opaque PSC

In our research, we first focused on the simulation of a $MAPbI_3$-based solar cell, utilizing TiO_2 as the electron transport layer (ETL) and Cu_2O as the hole transport layer (HTL). For the 400 nm thick opaque absorber configuration, the cell exhibited a V_{oc} of 1.23 V, a J_{sc} of 19.9 mA/cm^2, a fill factor (FF) of 83.77%, and an overall efficiency of 20.65%. However, when the absorber thickness was reduced to 200 nm, imbuing the structure with semitransparent properties, the V_{oc} slightly increased to 1.24 V. This can be attributed to reduced recombination in thinner layers, which can lead to a higher quasi-Fermi level split and, consequently, an enhanced V_{oc}. However, the J_{sc} showed a decline to 16.79 mA/cm^2, indicative of a decreased photon absorption in the thinner absorber layer. Despite this, the FF remained almost constant at 83.72%, and the efficiency reduced to 17.45%.

Substituting the absorber to toxic $FAPbI_3$, with the ETL and HTL remaining unchanged, and maintaining a 400 nm thickness yielded a V_{oc} of 1.16 V, J_{sc} of 23.9 mA/cm^2, FF of 83.69%, and an efficiency of 23.37%. When the thickness was adjusted to 200 nm, the V_{oc} increased to 1.18 V due to the aforementioned recombination

dynamics in thinner layers. The J_{sc}, however, declined to 19.00 mA/cm^2 due to diminished light absorption, but interestingly, the FF saw an improvement to 85.97%. This could result from a more uniform electric field distribution in the thinner absorber layer, facilitating enhanced charge collection. The net efficiency for this configuration stood at 19.46%.

Further exploration with a non-toxic $MAGeI_3$ absorber at 400 nm yielded a V_{oc} of 1.4 V, J_{sc} of 13.2 mA/cm^2, FF of 78.18%, and an efficiency of 14.59%. When reduced to a 200 nm thickness, the V_{oc} remained stable at 1.4 V. The J_{sc} however decreased to 9.9 mA/cm^2 due to a reduction in light harvesting capability of the thinner layer. The fill factor exhibited an upturn to 82.28%, possibly a result of improved charge transport in the thinner layer, leading to an overall efficiency of 11.55%.

Lastly, employing a non-toxic $RbGeI_3$ absorber at 400 nm, we observed a V_{oc} of 0.81 V, J_{sc} of 30.8 mA/cm^2, FF of 80.70%, and an efficiency of 20.40%. Altering the thickness to 200 nm saw the V_{oc} rising to 0.84 V, a phenomenon consistent with reduced recombination in thinner absorbers. The J_{sc} recorded a decline to 24.8 mA/cm^2 due to attenuated absorption. The FF remained stable at 80.70%, resulting in an efficiency of 17.03% for this configuration.

Table 2. Comparison of performance parameters of the opaque and semitransparent.

Structure	V_{oc}	J_{sc}	FF	Efficiency
TiO_2/$MAPbI_3$ (Opaque)/Cu_2O	1.23 V	19.9 mA/Cm^2	83.77	20.65 %
TiO_2/$MAPbI_3$ (Semitransparent)/Cu_2O	1.24 V	16.79 mA/Cm^2	83.72	17.45 %
TiO_2/$FAPbI_3$ (Opaque)/Cu_2O	1.16 V	23.9 mA/Cm^2	83.69	23.37 %
TiO_2/$FAPbI_3$ (Semitransparent)/Cu_2O	1.18 V	19.0 mA/Cm^2	85.97	19.46 %
TiO_2/$MAGeI_3$ (Opaque)/Cu_2O	1.4 V	13.2 mA/Cm^2	78.18	14.59 %
TiO_2/$MAGeI_3$ (Semitransparent)/Cu_2O	1.4 V	9.9 mA/Cm^2	82.28	11.55 %
TiO_2/$RbGeI_3$ (Opaque)/Cu_2O	0.81 V	30.8 mA/Cm^2	80.70	20.40 %
TiO_2/$RbGeI_3$ (Semitransparent)/Cu_2O	0.84 V	24.8 mA/Cm^2	80.70	17.03 %

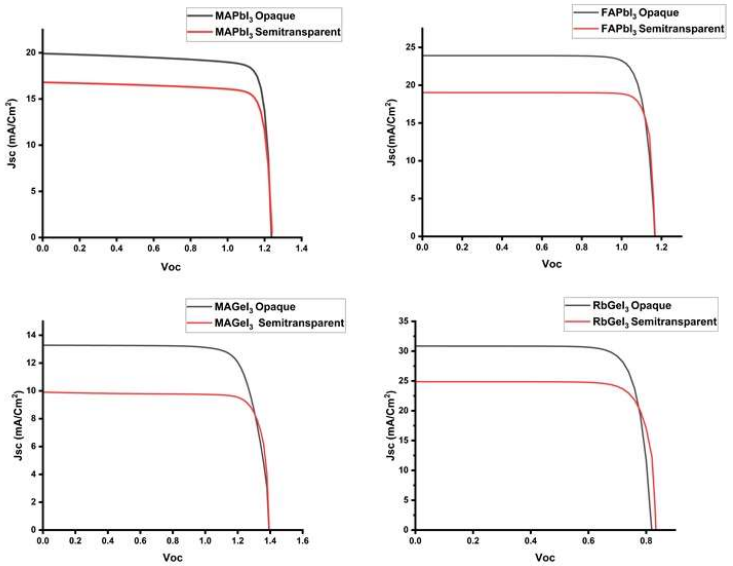

Figure 2. IV curve of toxic and non toxic perovskite solar cell opaque and semitransparent.

3.2. Effect of toxic PSC semitransparent and opaque on absorber thickness variation

The thickness of the absorber layer has a substantial impact on the efficiency and several other characteristics of the device [40,41]. In the investigations of toxic perovskite solar cells (PSC) using TiO_2 as the electron transport layer (ETL) and Cu_2O as the hole transport layer (HTL), it became evident that thickness variations profoundly influence the device's photo electronic properties. Specifically, when the absorber layers of $MAPbI_3$ and $FAPbI_3$ were set at thicknesses of 400 nm and 200 nm, nearly analogous performance metrics were recorded. One striking observation was the direct correlation between the thickness of the absorber layer and the short-circuit current density. With increasing thickness, a rise in J_{sc} was universally recorded across both semitransparent and opaque configurations of the PSCs. This trend is anticipated as a thicker absorber offers more substantial opportunity for photon absorption, subsequently leading to a heightened photo-generated carrier density. Notably, $FAPbI_3$ consistently manifested a superior J_{sc} when compared to $MAPbI_3$. The enhanced performance of $FAPbI_3$ can be rationalized by its broader absorption spectrum and superior charge carrier diffusion lengths, enabling it to capture and utilize photons more efficiently than $MAPbI_3$.

The observed decrease in V_{oc} with increasing thickness for both $MAPbI_3$ and $FAPbI_3$ perovskite solar cells is a phenomenon that aligns with established photovoltaic principles. In solar cells, V_{oc} is primarily influenced by the difference in quasi-Fermi levels, which is affected by recombination processes within the cell. As the absorber layer thickness increases, the likelihood of charge carriers recombining before reaching the electrodes also increases, leading to a reduction in V_{oc}. The increase in bulk recombination in thicker layers is a consequence of a longer path that charge carriers must traverse, which raises the probability of encountering defect sites. Interface recombination is similarly exacerbated as thicker films can promote a rougher interface due to increased grain size or a higher occurrence of pinholes, which disrupt the charge carrier extraction process. This is especially true for the interfaces between the perovskite layer and the charge transport layers, where imperfect contact can create additional energy barriers and trap states. The more significant decline in V_{oc} for $FAPbI_3$ compared to $MAPbI_3$ as thickness increases could stem from several factors. $FAPbI_3$ is known to have a different crystal structure compared to $MAPbI_3$, which might be more prone to defects, particularly when subjected to strain or other stressors common in thicker films. These defects may manifest as deep-level traps, exacerbating non-radiative recombination rates disproportionately in $FAPbI_3$. Additionally, the larger organic cation in $FAPbI_3$ could lead to a more complex crystallographic texture and less optimal grain structure when film thickness is increased. The inherent instability of $FAPbI_3$ under ambient conditions could also contribute to the higher defect density, as thicker layers are more difficult to completely convert to the desired perovskite phase without residual PbI_2 or other phases that can act as recombination centers. Furthermore, the ionic movement within the perovskite lattice could be more pronounced in $FAPbI_3$ with increased thickness, leading to ionic accumulation at the interfaces and the formation of additional recombination sites. The accumulation of such ionic defects at grain boundaries or at

the interface with charge transport layers can significantly impact the electronic properties of the perovskite layer, further impairing the V_{oc}.

Analyzing the fill factor (FF), it was discerned that, for $MAPbI_3$, an initial increase in FF with thickness plateaued and subsequently showed a decline. This behavior can be linked to improved charge extraction in moderately thick layers, countered by increased recombination events in excessively thick layers. The Fill Factor (FF) of $FAPbI_3$-based photovoltaic cells upon reducing the active layer thickness to 200 nm. Specifically, the FF improved from 83.69% to 85.97%. This notable increase can be attributed to a synergy of factors induced by the optimized layer thickness. Firstly, a thinner $FAPbI_3$ layer effectively reduces the path length for charge carrier diffusion. This decrease minimizes the likelihood of charge carrier recombination, a critical factor in enhancing charge collection efficiency. The shorter diffusion paths ensure a more efficient transport of electrons and holes to their respective electrodes, thereby improving the overall cell efficiency. Secondly, the optimized thickness enhances light harvesting capabilities. In thinner layers, light transmission is more efficient, with reduced losses due to reflection and absorption in the non-active layers of the cell. This improvement in light management directly translates to higher photocurrents, contributing to the observed increase in FF. Furthermore, electrical properties of the $FAPbI_3$ layer are also positively influenced by the reduced thickness. Thinner layers have been found to exhibit increased charge mobility and reduced series resistance, both of which are conducive to higher FF values. These electrical improvements are likely due to fewer defects and a more uniform crystalline structure in the thinner $FAPbI_3$ layer.

The observed trend of increasing efficiency with thicker absorber layers across both $MAPbI_3$ and $FAPbI_3$ perovskite solar cells can be comprehensively analyzed by considering the interplay between the three pivotal parameters of solar cell performance: J_{sc}, V_{oc}, and FF. Thickening the absorber layer typically enhances the optical path length within the solar cell, facilitating greater light absorption and, consequently, increasing the generation of electron-hole pairs. This directly contributes to an increase in J_{sc}, as there are more charge carriers available to contribute to current flow under short-circuit conditions. This effect is generally considered the primary driver for the observed rise in efficiency as the absorber layer's thickness increases. While a thicker layer boosts J_{sc}, the impact on V_{oc} and FF is more nuanced. V_{oc} can decrease with thicker layers due to the increased probability of recombination as carriers travel longer distances to reach the electrodes. However, the net effect on efficiency can still be positive if the gain in J_{sc} outweighs the loss in V_{oc}. The FF, which is a measure of the solar cell's quality and represents the 'squareness' of the current-voltage curve, can also be affected. A thicker layer may lead to higher series resistance and lower shunt resistance, potentially decreasing the FF. However, if the recombination can be managed and resistance optimized, the FF may not suffer significantly, thus contributing to the overall enhancement in efficiency. $FAPbI_3$ persistent superiority in efficiency over $MAPbI_3$ can be dissected into its inherent material advantages. $FAPbI_3$ typically exhibits higher absorption coefficients than $MAPbI_3$, meaning it can absorb the same amount of light in a thinner layer compared to $MAPbI_3$. This efficient use of photons can lead to better performance, especially in

thinner cells where the effects of recombination are less pronounced. Moreover, $FAPbI_3$ is often reported to have longer charge carrier lifetimes, which is a direct indicator of reduced recombination rates. Longer carrier lifetimes imply that the generated charge carriers can travel longer distances without recombining, which is particularly beneficial in thicker films where the distance to the electrode is greater. Nevertheless, $FAPbI_3$ is not without its limitations, such as potential instability and phase purity issues that can affect long-term performance. However, its high efficiencies in laboratory conditions suggest that when these limitations are managed, the intrinsic properties of $FAPbI_3$ lead to superior performance. This could be due to a more favorable bandgap for solar applications, or possibly due to better alignment with the transport layers, which can facilitate more efficient charge extraction. Both materials show improved efficiency with increased absorber thickness due to higher J_{sc}, $FAPbI_3$ inherent material properties, particularly its superior photon absorption and charge carrier dynamics, afford it a consistent edge in performance over $MAPbI_3$. The detailed interplay of these factors underlines the multifaceted considerations required to optimize perovskite solar cell efficiency.

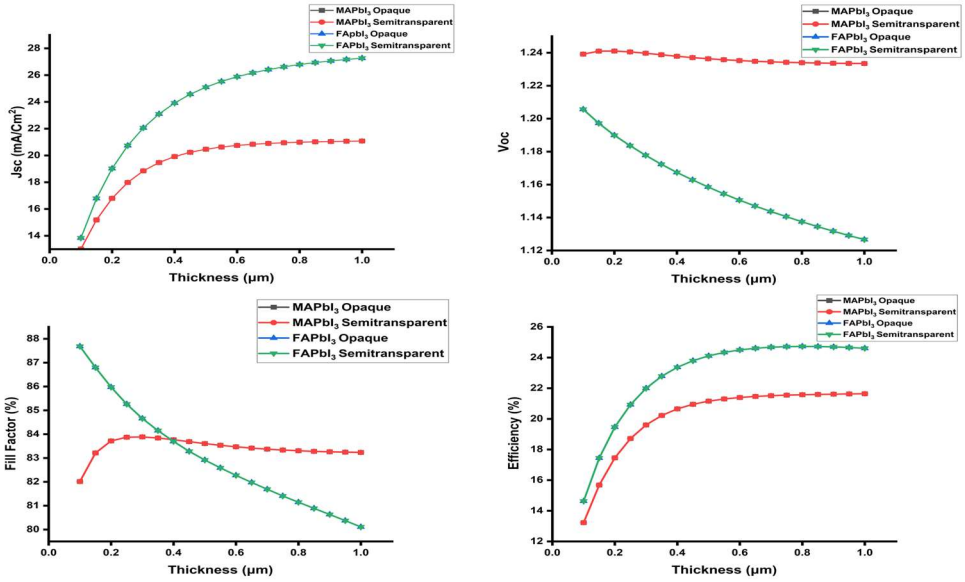

Figure 3. Effect of thickness variation on toxic PSC semitransparent and opaque.

3.3. Effect of non toxic PSC semitransparent and opaque on absorber thickness variation

The quantity of perovskites thickness has an effect on a material's lifespan, the length of time it takes for photo generated holes and electrons to diffuse, and both of those factors [42,43]. In our continued exploration of perovskite solar cells (PSC), emphasis was directed towards the non-toxic alternatives, specifically $MAGeI_3$ and $RbGeI_3$, with TiO_2 functioning as the electron transport layer (ETL) and Cu_2O as the hole transport layer (HTL). Intriguingly, preliminary simulations revealed comparable performance metrics for both $MAGeI_3$ and $RbGeI_3$ at thicknesses of 400 nm and 200 nm.

A noteworthy observation was the evident increase in J_{sc} with the augmentation of absorber layer thickness, spanning both semitransparent and opaque device

configurations. Such a trend is anticipated, as a denser absorber layer typically provides a larger domain for effective photon absorption, subsequently escalating the photo-generated carrier density. Despite this common trend, $RbGeI_3$ persistently exhibited a superior J_{sc} in comparison to $MAGeI_3$. This disparity can be elucidated by the broader absorption spectrum of $RbGeI_3$, combined with potential longer charge carrier diffusion lengths, culminating in its elevated proficiency in capturing and converting photons.

For V_{oc}, a shared trait between the two materials was a decrement with increasing absorber thickness. $RbGeI_3$, in particular, manifested a pronounced decline in V_{oc}. This can be attributed to the increased prevalence of bulk and interface recombination sites in thicker layers. The more significant V_{oc} diminution in $RbGeI_3$ might point towards its heightened defect density or a susceptibility to grain boundary imperfections that intensify recombination events with layer thickness.

The fill factor (FF) behavior in $RbGeI_3$, we observed a complex relationship between layer thickness and FF. Initially, as the layer thickness of $RbGeI_3$ increases, there is an ascent in FF. This initial increase can be attributed to enhanced charge extraction efficiency. At moderate thicknesses, the layer facilitates better charge transport to the electrodes, thereby improving the overall FF. This effect is primarily due to the reduced probability of charge recombination in the bulk of the material, as charges can be more effectively extracted before they have a chance to recombine. However, as the thickness continues to increase beyond this optimal range, the FF begins to decline. This decline in FF at higher thicknesses is due to the increased path length for charge carriers to travel to the electrodes. The longer distance increases the likelihood of charge carrier recombination before they can be effectively extracted. This increase in recombination events ultimately overshadows the benefits of improved charge extraction seen at moderate thicknesses, leading to a reduction in FF. In contrast, our findings with $MAGeI_3$ present a different scenario. With this material, we consistently observed a decline in FF as the layer thickness increased. This uniform decline suggests that the primary factor influencing FF in $MAGeI_3$ is not the improved charge extraction efficiency but rather an amplified rate of charge recombination. The increased thickness exacerbates this recombination, likely due to a higher density of defects or less favorable charge transport properties within the material. As a result, any potential benefits of enhanced charge extraction are negated by the dominant recombination processes, leading to a consistent decrease in FF with increasing layer thickness. Both $RbGeI_3$ and $MAGeI_3$ exhibit thickness-dependent FF behaviors, the underlying mechanisms differ. $RbGeI_3$ shows an optimal thickness range where FF peaks due to a balance between charge extraction and recombination, while $MAGeI_3$ consistently demonstrates a decrease in FF with increasing thickness, dominated by an increased recombination rate.

Efficiency metrics displayed an encouraging trend for both perovskites. With the bolstering of the absorber layer, a consistent enhancement in efficiency was observed for both $MAGeI_3$ and $RbGeI_3$. This progression can be comprehended as the cumulative outcome of the evolving J_{sc}, V_{oc} and FF dynamics. The augmentation in J_{sc}, due to the more substantial photon absorption in thicker layers, likely serves as a principal contributor to this trend.

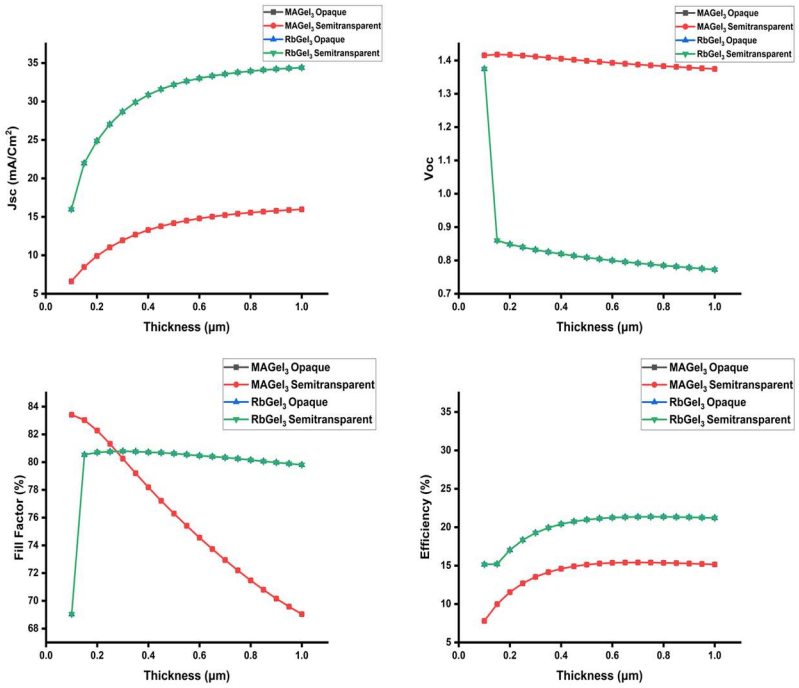

Figure 4. Effect of thickness variation on non toxic PSC semitransparent and opaque.

3.4. Effect of toxic PSC semitransparent and opaque on absorber doping variation

In our exploration of the intrinsic complexities of toxic perovskite solar cells (PSCs), particular attention was given to the subtleties arising from absorber doping variations. Through meticulous experimentation, several noteworthy trends emerged, underpinning the critical role of doping in modulating pivotal photovoltaic parameters.

The observed discrepancies in the J_{sc} between opaque and semitransparent configurations of $MAPbI_3$ and $FAPbI_3$ solar cells as doping concentrations were incremented warrants a comprehensive examination. Inherently, the opaque cells are designed with a thicker absorber layer, which inherently possesses a greater capacity for light harvesting. This structural characteristic facilitates enhanced photon absorption, leading to a higher rate of charge carrier generation when compared to their semitransparent counterparts. The increase in J_{sc} for opaque cells can be directly correlated to their improved light absorption properties. The thicker absorptive layers in these cells are more efficient at converting incident photons into photo-generated electrons and holes, resulting in an increased number of charge carriers available for current generation. Consequently, as doping levels are elevated, the opaque cells maintain superior J_{sc} values by virtue of their robust light-absorbing capabilities. However, the data indicates a decline in J_{sc} beyond specific doping thresholds, suggesting the onset of deleterious effects due to excessive doping. High dopant concentrations can lead to the formation of new defect states within the perovskite crystal structure. These defects can act as recombination centers for electrons and holes, effectively reducing the lifetime of charge carriers and diminishing the J_{sc}. Moreover, excessive doping can perturb the crystallinity of the perovskite layer, leading to increased grain boundary scattering and non-radiative recombination events,

further impeding the J_{sc}. Additionally, in highly doped regimes, the surplus dopants can create a detrimental band tailing effect. This effect introduces states within the bandgap that trap charge carriers, effectively reducing the number of free carriers that contribute to the J_{sc}. Such trap states can exacerbate non-radiative recombination, particularly if the traps are deep within the bandgap and difficult for carriers to escape. Therefore, while opaque configurations of PSCs inherently present an advantage in J_{sc} due to their light absorption proficiency, there exists a critical doping limit beyond which the benefits of additional doping are overshadowed by the onset of recombination and charge trapping phenomena. This delicate interplay between dopant concentration and cell architecture underscores the necessity for judicious dopant management to optimize the J_{sc} and, by extension, the overall efficiency of perovskite solar cells.

The stability of the V_{oc} across varying doping levels up to E15 suggests an initial doping concentration range where the intrinsic material properties of both $MAPbI_3$ and $FAPbI_3$ structures are not significantly perturbed. In photovoltaic materials, V_{oc} is predominantly determined by the quasi-Fermi level separation, which can be influenced by the recombination rate of charge carriers within the cell. The plateau in V_{oc} implies that up to this doping threshold, the rate of recombination does not substantially increase, possibly due to a balance between defect passivation and the introduction of new defect states by doping. The sudden escalation in V_{oc} observed at the E15 doping concentration for both opaque and semitransparent structures of $MAPbI_3$ and $FAPbI_3$ indicates a threshold beyond which additional doping begins to decisively suppress non-radiative recombination processes. This could result from a more pronounced passivation of deep-level defects that act as recombination centers. High dopant densities may saturate these defect sites, leading to a reduction in their recombination activity which is one of the major contributors to voltage losses in PSCs. Furthermore, the rise in V_{oc} could also be attributed to an improved charge carrier separation and extraction efficiency. At optimal doping levels, the charge carriers' lifetime increases, allowing for a greater probability of extraction before recombination can occur. The increase in V_{oc} at E15 may also be a reflection of improved electronic properties such as increased carrier mobility or reduced trap-assisted recombination, which are conducive to higher V_{oc} values. The observed trend of increasing V_{oc} at higher doping concentrations points to a complex interaction where the dopants not only passivated existing defects but may also alter the electronic landscape of the perovskite material, enhancing the overall energy conversion efficiency of the cells. Such an effect would be critical in the push for higher-efficiency PSCs, as V_{oc} is a direct contributor to the power conversion efficiency. These results underscore the need for a careful balance in doping strategies to optimize the photovoltaic parameters and achieve maximum efficiency in perovskite solar cells.

The fill factor (FF) dynamics, in relation to doping variations, sketched an intricate narrative. An initial drop in FF values was discerned, culminating in a trough at the E15 doping level. Surprisingly, post this nadir, FF values embarked on a rejuvenation path. This trajectory can be conceptualized considering the balance between the beneficial effects of increased charge carrier density and the potential setbacks of escalated recombination events. The inflection at E15 might be indicative

of a transient regime where increased doping-induced defects or grain boundary disruptions momentarily outweigh the advantages brought about by enhanced charge carrier populations. However, as doping is further intensified, a more conducive charge transport environment might manifest, possibly through improved grain connectivity or lattice ordering, culminating in the observed FF uptrend.

In the efficiency performance of $FAPbI_3$ opaque cells, the observed dip in efficiency at the E15 doping level warrants a detailed analysis. Scientifically, this anomaly could be attributed to a threshold in doping concentration that temporarily disrupts the crystalline order or introduces defect states, which act as recombination centers, thus momentarily impeding charge carrier lifetimes and reducing efficiency. As doping concentration increases beyond E15 to E18, the efficiency recovers and continues to rise, suggesting a passivation of these defects or a shift in the Fermi level that enhances charge carrier extraction. The $FAPbI_3$ semitransparent cells exhibit a similar pattern, where the dip at E15 followed by a subsequent rise in efficiency could be indicative of a complex interplay between light absorption and electrical properties. At E15, the increased doping might initially lead to suboptimal band alignment, adversely affecting charge transport. However, further doping appears to optimize the band structure or improve the electronic quality of the perovskite layer, thereby increasing the efficiency as observed. For $MAPbI_3$ opaque cells, the slight dip in efficiency seen up to the E15 doping level can be rationalized by considering the doping-induced perturbations in the perovskite film morphology or the interface with charge transport layers. Such perturbations could momentarily hinder the charge collection efficiency. Upon increasing the doping beyond E15, the efficiency trend suggests an amelioration of these effects, possibly due to improved interfacial contact or electronic passivation that enhances charge transport and collection. In contrast, the $MAPbI_3$ semitransparent cells demonstrate an efficiency raise post E15 doping. This improvement could be associated with enhanced light management within the cell due to the modified electronic properties of the perovskite layer at higher doping levels, which aids in superior charge generation and collection. Integrating these observations, it can be postulated that the doping concentration acts as a dual edged sword, with the potential to either introduce electronic and structural disruptions or to enhance the photovoltaic performance by modulating the optoelectronic properties of the perovskite material. The E15 doping level emerges as a critical juncture where the interdependence of these effects is most pronounced, and beyond which the PSCs tend to exhibit.

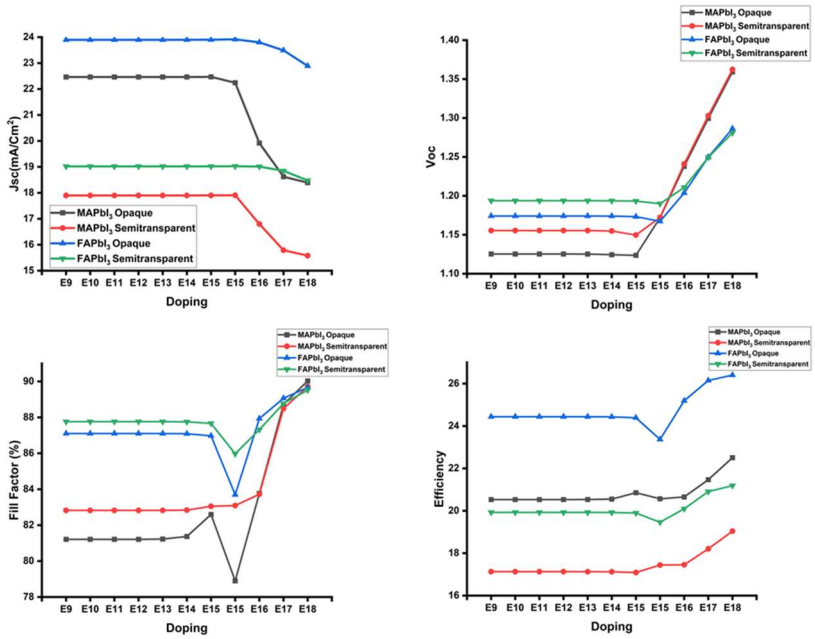

Figure 5. Effect of doping variation on toxic PSC semitransparent and opaque.

3.5. Effect of nontoxic PSC semitransparent and opaque on absorber doping variation

In our continued quest to probe the intricacies of perovskite solar cells (PSCs), focus was shifted towards the non-toxic variants, specifically $MAGeI_3$ and $RbGeI_3$. Intriguingly, the behavior displayed by these materials, especially in response to absorber doping variations, exhibited marked divergences from their toxic counterparts, underscoring the nuances of non-toxic PSCs.

A cursory look at the J_{sc} trends divulged that as doping concentrations swelled, both $MAGeI_3$ and $RbGeI_3$ remained remarkably steadfast, showing no significant perturbations in J_{sc}. This stoic response can potentially be attributed to an equilibrium struck between enhanced photo-generation of charge carriers and an increase in non-radiative recombination events at augmented doping levels. However, at the E17 doping concentration, a dichotomous behavior was observed for $MAGeI_3$; while the opaque structure recorded an uptick in J_{sc}, its semitransparent counterpart delineated a decline. This can likely be ascribed to disparate light absorption and scattering profiles inherent to the two configurations, with the opaque structure possibly benefiting from a thicker absorber layer, facilitating more efficient photon absorption.

The stability of the V_{oc} across a range of doping concentrations for $MAGeI_3$ solar cells suggests an optimal electronic environment for charge carrier separation under most doping conditions. V_{oc} is inherently linked to the potential difference created by the separation of photogenerated electrons and holes; a stable V_{oc} across varying doping levels implies a well-maintained balance between charge generation and recombination processes. However, the noted downturn in V_{oc} at the E17 doping concentration suggests a perturbation in this balance. An increase in recombination events at this doping level could be due to several mechanisms. Firstly, excessive doping may lead to an oversaturation of the perovskite lattice with foreign atoms, which could disrupt the crystal structure and create new defect states. These defects

often serve as recombination centers that facilitate the annihilation of charge carriers, thereby diminishing the V_{oc}. Secondly, the introduction of a high concentration of dopant atoms could alter the perovskite's electronic properties, such as the bandgap or the effective masses of charge carriers, which might also contribute to the decreased V_{oc}. In contrast, the V_{oc} trends for $RbGeI_3$ demonstrate a different behavior with a resurgence in V_{oc} values post the E15 doping level, indicative of an improved photovoltaic performance. This could be attributed to the dopants acting as beneficial modifiers of the perovskite lattice. The dopants may occupy interstitial sites or substitute for germanium or iodide ions, leading to improved lattice ordering and stabilization. Such improvements could reduce the density of defect states within the bandgap that are responsible for non-radiative recombination, thereby increasing the V_{oc}. Additionally, the resurgence in V_{oc} could also be a manifestation of enhanced electronic quality of the perovskite layer, where dopants passivate surface and bulk defects. By neutralizing these charge trap sites, the recombination kinetics are altered favorably, leading to an extended charge carrier lifetime and thus, a higher V_{oc}. Moreover, the dopants might induce a shift in the energy levels at the perovskite interfaces, promoting better energy level alignment with the adjacent transport layers. This improved alignment facilitates more efficient charge extraction, thereby contributing to the increase in V_{oc} observed.

The narrative took another twist when assessing the fill factor (FF). For $MAGeI_3$, the opaque structure at E17 registered a conspicuous drop in FF, suggesting increased series resistance or potential issues with charge extraction. Interestingly, the semitransparent variant remained relatively unscathed. In parallel, $RbGeI_3$, post the E15 doping concentration, witnessed an uplift in FF for both configurations. This could underscore the establishment of a more conducive charge transport environment, potentially stemming from enhanced grain connectivity or reduced interface recombination.

Efficiency trends for $MAGeI_3$ revealed a subdued descent up to E17 for both configurations, hinting at the combined effects of the evolving V_{oc} and J_{sc} trends. $RbGeI_3$, on the other hand, unveiled an efficiency ascent post-E15, with the opaque structure consistently outperforming its semitransparent counterpart. This likely reiterates the benefits of a denser absorber layer in the opaque configuration, affording more efficient photon management and charge extraction.

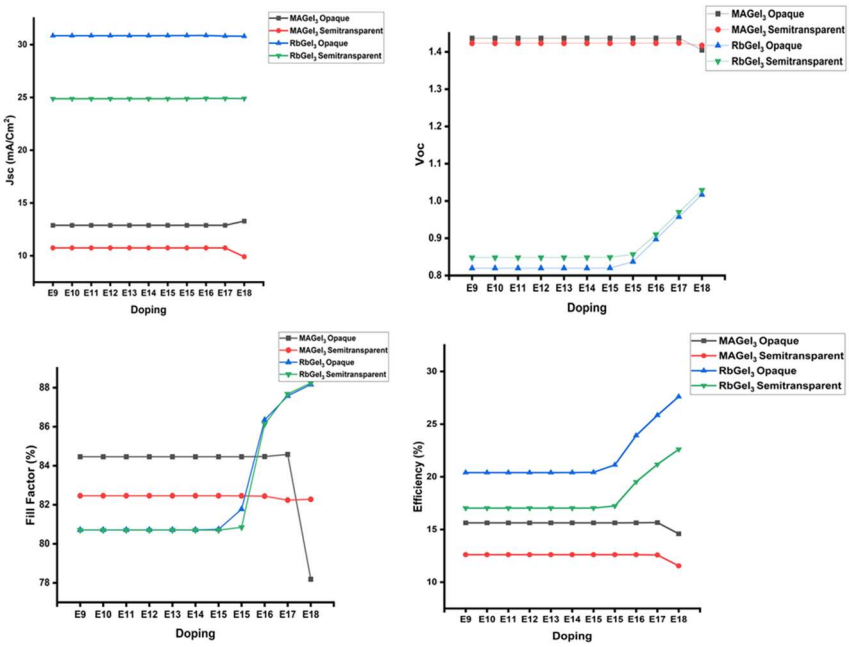

Figure 6. Effect of doping variation on non toxic PSC semitransparent and opaque.

4. Conclusion

In conclusion, the promise of perovskite solar cells (PSCs) in modern sustainable energy solutions is undeniable. Our comprehensive research delves deep into the performance metrics of both toxic and non-toxic PSCs, shedding light on their suitability for various applications, including Building-Integrated Photovoltaics (BIPV). Commencing with the $MAPbI_3$-based solar cell, leveraging the synergies of TiO_2 and Cu_2O as ETL and HTL, respectively, a 400 nm opaque absorber delivered a laudable efficiency of 20.65%. Venturing into a semitransparent structure with a reduced thickness of 200 nm, salient changes were observed, notably a mild uptick in V_{oc} and a drop in J_{sc}. This semitransparent design holds immense potential for BIPV applications, harmonizing solar energy harnessing with architectural aesthetics. Substituting the absorber with the toxic $FAPbI_3$, while retaining the ETL and HTL configuration, resulted in an efficiency of 23.37% for the 400 nm opaque setup. Transitioning to the semitransparent 200 nm configuration, we once again noted a heightened V_{oc} and a constricted J_{sc}. The perseverance of the fill factor at this thickness might suggest superior potential in BIPV, providing a balance between transparency and performance. Turning our attention to the non-toxic $MAGeI_3$ variant at 400 nm, an efficiency of 14.59% was achieved. As with previous configurations, migrating to the 200 nm semitransparent setup introduced expected trends – consistent V_{oc} but declining J_{sc} and overall efficiency. The unique properties of $MAGeI_3$ within a semitransparent construct present exciting prospects, particularly in BIPV scenarios where transparency without significant compromise in efficiency is desired. Our exploration with the non-toxic $RbGeI_3$ at 400 nm yielded an efficiency of 20.40%. However, transitioning to its 200 nm semitransparent counterpart resulted in the familiar patterns of enhanced V_{oc} but reduced J_{sc}. The promise of such configurations in BIPV applications cannot be understated, especially considering the delicate balance between aesthetics and functionality they offer. This research not only

provides insights into the nuanced behavior of PSCs across different absorbers and thicknesses but also underscores the promising potential of semitransparent configurations in BIPV applications. The trade-offs between efficiency, aesthetics, and transparency necessitate continued research in this domain, and our study stands as a pivotal step in this ongoing journey.

Author contributions: Conceptualization, AHHK and AB; methodology, HU, AHHK and LPL; software, AHHK and AB; validation, AHHK and ADK; formal analysis, AHHK, ADK and LL; investigation, AHHK and KB; resources, AHHK and SK; data curation, AHHK and ADK; writing—original draft preparation, AHHK, ADK and SK; writing—review and editing, AHHK, ADK and SK; visualization, AHHK, HU and AB; supervision, ADK and SK; project administration, AHHK, ADK, AB and SK; funding acquisition, ADK. All authors have read and agreed to the published version of the manuscript.

Conflict of interest: The authors declare no conflict of interest.

References

1. Kojima A, Teshima K, Shirai Y, et al. Organometal halide perovskites as visible-light sensitizers for photovoltaic cells. Journal of the American Chemical Society. 2009, 131(17): 6050–6051. doi: 10.1021/ja809598r
2. Park NG. Organometal perovskite light absorbers toward a 20% efficiency low-cost solid-state mesoscopic solar cell. The Journal of Physical Chemistry Letters. 2013, 4(15): 2423–2429. doi: 10.1021/jz400892a
3. Snaith HJ. Perovskites: The emergence of a new era for low-cost, high-efficiency solar cells. The Journal of Physical Chemistry Letters. 2013, 4(21): 3623–3630. doi: 10.1021/jz4020162
4. Sun S, Salim T, Mathews N, et al. The origin of high efficiency in low-temperature solution-processable bilayer organometal halide hybrid solar cells. Energy & Environmental Science. 2014, 7(1): 399–407. doi: 10.1039/c3ee43161d
5. Stranks SD, Eperon GE, Grancini G, et al. Electron-hole diffusion lengths exceeding 1 micrometer in an organometal trihalide perovskite absorber. Science. 2013, 342(6156): 341–344. doi: 10.1126/science.1243982
6. Khan AHH, Basit S, Hameedullah. Improving the efficiency of lead-free non-toxic rubidium germanium iodide perovskite solar cell using a molybdenum disulfide interface layer: A SCAPS 1D simulation study. International Research Journal of Modernization in Engineering Technology and Science. 2023; 5(10): 1801–1804. doi: 10.56726/IRJMETS45496
7. Barrows AT, Pearson AJ, Kwak CK, et al. Efficient planar heterojunction mixed-halide perovskite solar cells deposited via spray-deposition. Energy & Environmental Science. 2014, 7(9): 2944–2950. doi: 10.1039/c4ee01546k
8. Vak D, Hwang K, Faulks A, et al. 3D printer based slot-die coater as a lab-to-fab translation tool for solution-processed solar cells. Advanced Energy Materials. 2014, 5(4). doi: 10.1002/aenm.201401539
9. Kim JH, Williams ST, Cho N, et al. Enhanced environmental stability of planar heterojunction perovskite solar cells based on blade-coating. Advanced Energy Materials. 2014, 5(4). doi: 10.1002/aenm.201401229
10. NREL. Best research-cell efficiency chart. Available online: https://www.nrel.gov/pv/cell-efficiency.html (accessed on 22 December 2023).
11. Li C, Lu X, Ding W, et al. Formability of ABX 3 (X = F, Cl, Br, I) halide perovskites. Acta Crystallographica Section B Structural Science. 2008, 64(6): 702–707. doi: 10.1107/s0108768108032734
12. Eperon GE, Stranks SD, Menelaou C, et al. Formamidinium lead trihalide: A broadly tunable perovskite for efficient planar heterojunction solar cells. Energy & Environmental Science. 2014, 7(3): 982. doi: 10.1039/c3ee43822h
13. Ono LK, Juarez-Perez EJ, Qi Y. Progress on perovskite materials and solar cells with mixed cations and halide anions. ACS Applied Materials & Interfaces. 2017, 9(36): 30197–30246. doi: 10.1021/acsami.7b06001
14. Saliba M, Matsui T, Seo JY, et al. Cesium-containing triple cation perovskite solar cells: Improved stability, reproducibility and high efficiency. Energy & Environmental Science. 2016, 9(6): 1989–1997. doi: 10.1039/c5ee03874j
15. Pellet N, Gao P, Gregori G, et al. Mixed-organic-cation perovskite photovoltaics for enhanced solar-light harvesting. Angewandte Chemie International Edition. 2014, 53(12): 3151–3157. doi: 10.1002/anie.201309361

16. Park NG. Perovskite solar cells: An emerging photovoltaic technology. Materials Today. 2015, 18(2): 65–72. doi: 10.1016/j.mattod.2014.07.007
17. De Wolf S, Holovsky J, Moon SJ, et al. Organometallic halide perovskites: Sharp optical absorption edge and its relation to photovoltaic performance. The Journal of Physical Chemistry Letters. 2014, 5(6): 1035–1039. doi: 10.1021/jz500279b
18. Chang YH, Park CH, Matsuishi K. First-principles study of the structural and the electronic properties of the lead-Halide-based inorganic-organic perovskites (CH~ 3NH~ 3) PbX~ 3 and CsPbX~ 3 (X= Cl, Br, I). Journal-Korean Physical Society. 2004; 44: 889–893.
19. Kulkarni SA, Baikie T, Boix PP, et al. Band-gap tuning of lead halide perovskites using a sequential deposition process. Journal of Materials Chemistry A. 2014, 2(24): 9221–9225. doi: 10.1039/c4ta00435c
20. Ding G, Zheng Y, Xiao X, et al. Sustainable development of perovskite solar cells: Keeping a balance between toxicity and efficiency. Journal of Materials Chemistry A. 2022, 10(15): 8159–8171. doi: 10.1039/d2ta00248e
21. Liu M, Johnston MB, Snaith HJ. Efficient planar heterojunction perovskite solar cells by vapour deposition. Nature. 2013, 501(7467): 395–398. doi: 10.1038/nature12509
22. Burschka J, Pellet N, Moon SJ, et al. Sequential deposition as a route to high-performance perovskite-sensitized solar cells. Nature. 2013, 499(7458): 316–319. doi: 10.1038/nature12340
23. Chen C, Kang H, Hsiao S, et al. Efficient and uniform planar-type perovskite solar cells by simple sequential vacuum deposition. Advanced Materials. 2014, 26(38): 6647–6652. doi: 10.1002/adma.201402461
24. Schneider A, Alon S, Etgar L. Evolution of photovoltaic performance in fully printable mesoscopic carbon-based perovskite solar cells. Energy Technology. 2019, 7(7). doi: 10.1002/ente.201900481
25. U.S. Energy Information Administration. Residential energy consumption survey (RECS). Available online: https://www.eia.gov/consumption/residential/ (accessed on 22 December 2023).
26. Zhang W, Anaya M, Lozano G, et al. Highly efficient perovskite solar cells with tunable structural color. Nano Letters. 2015, 15(3): 1698–1702. doi: 10.1021/nl504349z
27. Xue Q, Xia R, Brabec CJ, et al. Recent advances in semi-transparent polymer and perovskite solar cells for power generating window applications. Energy & Environmental Science. 2018, 11(7): 1688–1709. doi: 10.1039/c8ee00154e
28. Jeon NJ, Na H, Jung EH, et al. A fluorene-terminated hole-transporting material for highly efficient and stable perovskite solar cells. Nature Energy. 2018, 3(8): 682–689. doi: 10.1038/s41560-018-0200-6
29. Shen H, Duong T, Peng J, et al. Mechanically-stacked perovskite/CIGS tandem solar cells with efficiency of 23.9% and reduced oxygen sensitivity. Energy & Environmental Science. 2018, 11(2): 394–406. doi: 10.1039/c7ee02627g
30. Service RF. Perovskite solar cells gear up to go commercial. Science. 2016, 354(6317): 1214–1215. doi: 10.1126/science.354.6317.1214
31. Della Gaspera E, Peng Y, Hou Q, et al. Ultra-thin high efficiency semitransparent perovskite solar cells. Nano Energy. 2015, 13: 249–257. doi: 10.1016/j.nanoen.2015.02.028
32. Imran H, Durrani I, Kamran M, et al. High-performance bifacial perovskite/silicon double-tandem solar cell. IEEE Journal of Photovoltaics. 2018, 8(5): 1222–1229. doi: 10.1109/jphotov.2018.2846519
33. Ball JM, Stranks SD, Hörantner MT, et al. Optical properties and limiting photocurrent of thin-film perovskite solar cells. Energy & Environmental Science. 2015, 8(2): 602–609. doi: 10.1039/c4ee03224a
34. Lie S, Bruno A, Wong LH, et al. Semitransparent perovskite solar cells with > 13% efficiency and 27% transperancy using plasmonic Au nanorods. ACS Applied Materials & Interfaces. 2022, 14(9): 11339–11349. doi: 10.1021/acsami.1c22748
35. Burgelman M, Nollet P, Degrave S. Modelling polycrystalline semiconductor solar cells. Thin Solid Films. 2000, 361–362: 527–532. doi: 10.1016/s0040-6090(99)00825-1
36. Raoui Y, Ez-Zahraouy H, Tahiri N, et al. Performance analysis of $MAPbI_3$ based perovskite solar cells employing diverse charge selective contacts: Simulation study. Solar Energy. 2019, 193: 948–955. doi: 10.1016/j.solener.2019.10.009
37. Karthick S, Velumani S, Bouclé J. Experimental and SCAPS simulated formamidinium perovskite solar cells: A comparison of device performance. Solar Energy. 2020, 205: 349–357. doi: 10.1016/j.solener.2020.05.041
38. Tariq Jan S, Noman M. Influence of layer thickness, defect density, doping concentration, interface defects, work function, working temperature and reflecting coating on lead-free perovskite solar cell. Solar Energy. 2022, 237: 29–43. doi: 10.1016/j.solener.2022.03.069
39. Pindolia G, Shinde SM, Jha PK. Optimization of an inorganic lead free RbGeI3 based perovskite solar cell by SCAPS-1D simulation. Solar Energy. 2022, 236: 802–821. doi: 10.1016/j.solener.2022.03.053

40. Tara A, Bharti V, Sharma S, et al. Device simulation of $FASnI_3$ based perovskite solar cell with $Zn(O_{0.3}, S_{0.7})$ as electron transport layer using SCAPS-1D. Optical Materials. 2021, 119: 111362. doi: 10.1016/j.optmat.2021.111362
41. Son DY, Im JH, Kim HS, et al. 11% efficient perovskite solar cell based on ZnO nanorods: An effective charge collection system. The Journal of Physical Chemistry C. 2014, 118(30): 16567–16573. doi: 10.1021/jp412407j
42. Barbé J, Tietze ML, Neophytou M, et al. Amorphous Tin oxide as a low-temperature-processed electron-transport layer for organic and hybrid perovskite solar cells. ACS Applied Materials & Interfaces. 2017, 9(13): 11828–11836. doi: 10.1021/acsami.6b13675
43. Kim H, Lim KG, Lee TW. Planar heterojunction organometal halide perovskite solar cells: Roles of interfacial layers. Energy & Environmental Science. 2016, 9(1): 12–30. doi: 10.1039/c5ee02194d